J. Fluid Mech. (1991), *vol.* 227, *pp.* 567–586
Printed in Great Britain

Experimental study of directional solidification of aqueous ammonium chloride solution

By C. F. CHEN AND FALIN CHEN†
Department of Aerospace and Mechanical Engineering, University of Arizona, Tucson, AZ 85721, USA

(Received 10 August 1989 and in revised form 15 December 1990)

Directional solidification experiments have been carried out using the analogue casting system of NH_4Cl-H_2O solution by cooling it from below with a constant-temperature surface ranging from −31.5 °C to +11.9 °C. The NH_4Cl concentration was 26% in all solutions, with a liquidus temperature of 15 °C. It was found that finger convection occurred in the fluid region just above the mushy layer in all experiments. Plume convection with associated chimneys in the mush occurred in experiments with bottom temperatures as high as +11.0 °C. However, when the bottom temperature was raised to +11.9 °C, no plume convection was observed, although finger convection continued as usual. A method has been devised to determine the porosity of the mush by computed tomography. Using the mean value of the porosity across the mush layer and the permeability calculated by the Kozeny–Carman relationship, the critical solute Rayleigh number across the mush layer for onset of plume convection was estimated to be between 200 and 250.

1. Introduction

Directional solidification is a process in which an alloy melt is solidified by cooling from the bottom of the mould. In the resulting casting, the grain boundaries transverse to the solidification direction are virtually eliminated. The material thus obtained shows increased creep rupture strain and improved thermal fatigue behaviour, two important characteristics for modern gas turbine blades. A general description of the process and the mechanical properties that can be achieved in these castings are given by McLean (1983). More recently, Kear (1986), in an article on advanced metals, presented a colourful illustration of the directional solidification process and the finished turbine blades etched to show the grain boundaries.

Under some circumstances, however, there are defects in the castings in the form of solute-rich, columnal regions extending longitudinally in the direction of the solidification. These are known as freckles, and their presence causes a deleterious effect on the strength of the castings. Giamei & Kear (1970) found the presence of freckles in directionally solidified castings of nickel-base superalloys and in binary nickel–aluminium alloys. Although the general mechanism for the onset of freckles is known to arise from compositional buoyancy forces resulting from interactions of fluid dynamical and thermodynamical effects in the combined region of the mushy and melt zones, the precise mechanism is not clearly understood at present, nor is there a method by which we can predict the onset of such occurrences and the areal

† Present address: The Institute of Applied Mechanics, National Taiwan University, Taipei, Taiwan, 10764 ROC.

distribution of the freckles (see reviews by Fisher 1981 and by Glicksman, Coriell & McFadden 1986).

During directional solidification of alloys with sufficiently high solutal concentrations, the planar freezing surface is morphologically unstable (Mullins & Sekerka 1964) and solidification is dendritic. As a result, the melt is separated from the eutectic solid by a region consisting of solid dendrites and interdendritic liquid, generally referred to as the mushy zone. Freckles, or channel segregates, are the result of plumes containing solute-rich liquid issuing from isolated chimneys in the mushy zone. These were first observed by McDonald & Hunt (1969) in a NH_4Cl-H_2O system being cooled from the side and the bottom. Jackson *et al.* (1966) seem to be the first group to use the transparent NH_4Cl-H_2O solution as an analogue system to study the solidification phenomenon of metallic alloys. McDonald & Hunt (1970) demonstrated conclusively that the onset of plumes is due to the fact that the solution rejected by solidification is lighter than the bulk fluid. Copley *et al.* (1970) used liquid nitrogen to solidify from below a 30-wt% NH_4Cl-H_2O solution in a transparent cylinder. After the mushy zone was well established, they were able to observe buoyant liquid jets issuing from chimneys which were irregularly spaced in the mush. The observation was possible because of the smaller index of refraction of the liquid in the plume due to its lower concentration of NH_4Cl than that in the bulk fluid. Associated with each jet was a buildup of crystals around the exit from the mush, marking each chimney with a conical mount at the mush–liquid interface. This is due to crystallization of solute-rich fluid being induced by the plume to flow toward the comparatively cool region near the exit of the plume. They were the first authors to attribute the onset of freckles to salt-finger convection.

Sample & Hellawell (1984) carried out further experiments with the NH_4Cl-H_2O solution. After isolated chimney–plume systems were well established, they were able to generate new plumes by withdrawing liquid very close to the freezing front (1 to 2 mm). They chilled the mould by using liquid nitrogen similar to the procedure carried out by Copley *et al.* (1970). However, plumes may be generated in NH_4Cl-H_2O systems using a much slower cooling rate. In connection with their study of the dynamics and energetics of the Earth's core, Roberts & Loper (1983) performed similar experiments by chilling the bottom of the mould with crushed ice and rock salt, achieving a temperature of -10 °C to -20 °C. The occurrence of the mushy zone and the subsequent onset of the chimney–plume system were similarly observed. In the same paper, Roberts & Loper presented a simple steady-state analysis of the mushy zone. More recently, Sarazin & Hellawell (1988) performed experiments in Pb-Sn, Pb-Sb, and Pb-Sn-Sb alloys and showed that some freckles may start and end within the ingot, indicating that as the solidification proceeds upward fluid dynamical and thermodynamical conditions are continuously changing and eventually some freckles are no longer viable.

Theoretical aspects of this problem have been considered by Hills, Loper & Roberts (1983), Fowler (1985), Huppert & Worster (1985), and Worster (1986). In all these efforts, the fluid rejected by solidification is assumed to be heavier than the melt in the bulk. The effect of convection was excluded. In the last few years, a number of computational schemes have appeared that take into account compositional as well as thermal convection in the combined liquid and mushy zone during directional solidification. Among these are Bennon & Incropera (1987), Beckermann & Viskanta (1988), and Heinrich (1988).

In this paper, we report the results of a series of experiments on directional solidification of a 26% NH_4Cl-H_2O solution cooled from below at temperatures

ranging from −31.5 °C to +11.9 °C. Plume convection existed in all experiments with bottom temperatures as high as 11.0 °C. However, when the bottom temperature was set at 11.9 °C, no plume convection occurred, although finger convection continued as usual due to the crystallization process. The flow in the fluid is illustrated by a number of shadowgraphs, and that in the mush by dye pictures. By using the computed tomography technique, the porosity of the mush was determined. Using an estimated value of the permeability based on the measured porosity, the critical solute Rayleigh number for the onset of plume convection was estimated to be between 200 and 250.

2. Experimental equipment and procedure

Results reported in this paper were obtained in two different laboratories, initiated at the Department of Applied Mathematics and Theoretical Physics, University of Cambridge, and continued in the AME Department of the University of Arizona.

The test tank used in Cambridge was 12.7 cm square and 38.1 cm tall. The four sides were made of Plexiglas for easy viewing, and the bottom was made of stainless steel. The tank was cooled from the bottom by placing it on a circular cooling plate made of brass which was approximately 30 cm in diameter and 2.54 cm thick. Antifreeze fluid cooled by a refrigerated circulator was pumped through the passage provided within the cooling plate to maintain it at a lower temperature. The system was capable of reaching −30 °C. A thermistor was inserted into an aluminium plate to obtain the temperature of the bottom of the tank. The tank was initially filled with 26% NH_4Cl-H_2O solution, and the cooling plate cooled to a predetermined temperature. The experiment was started when the test tank was placed on top of the cooling plate.

In Tucson, the experiments were conducted in a similar tank, except the bottom was made of brass. The cooling plate, which was also made of brass, was square, had the same dimensions as the bottom of the tank, and was 2.54 cm thick. In addition to the thermocouple installed in the bottom plate of the tank, a heat flux meter was installed between the bottom of the tank and the cooling plate. A thermocouple frame, made of a Plexiglas cylinder, was provided so that temperatures at different levels could be monitored. Before each experiment, the test tank containing 26% NH_4Cl-H_2O solution was placed on top of the square cooling plate. The coolant in the refrigerated circulator was cooled to a preselected temperature. The experiment was started when appropriate valves were adjusted to allow the coolant to flow through the passage provided in the cooling plate. The tank bottom was cooled very rapidly, as shown in figure 1, for experiment S11 in which the final bottom temperature was −14.3 °C and the initial fluid temperature was 24.6 °C. The time constant was 1.8 min, and the final bottom temperature was reached at 15 min. This is typical of all experiments conducted.

3. General observations of the flow process in the bulk fluid

According to the phase diagram of the aqueous solution of NH_4Cl shown in figure 2, the liquidus temperature for a 26% NH_4Cl-H_2O solution is +15 °C; the eutectic concentration is 19.7% NH_4Cl and is formed at −15.4 °C. A total of 14 experiments were carried out with nominal bottom temperatures, T_B, at −30 °C, −15 °C, −10 °C, −5 °C, 0 °C, 5 °C, 10 °C, 11 °C, and 12 °C. These are shown as black dots along the 26% line in figure 3. A list of all experiments and their experimental conditions is

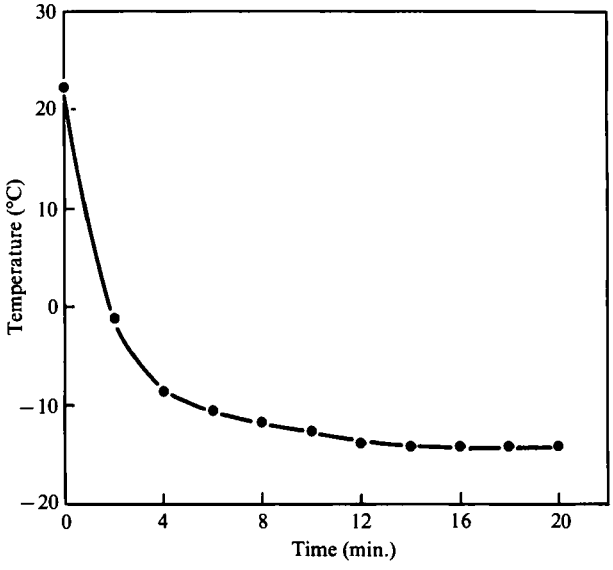

FIGURE 1. Temperature of the tank bottom during the first 20 min. of cooling for experiment S11 with $T_B = -14.3$ °C.

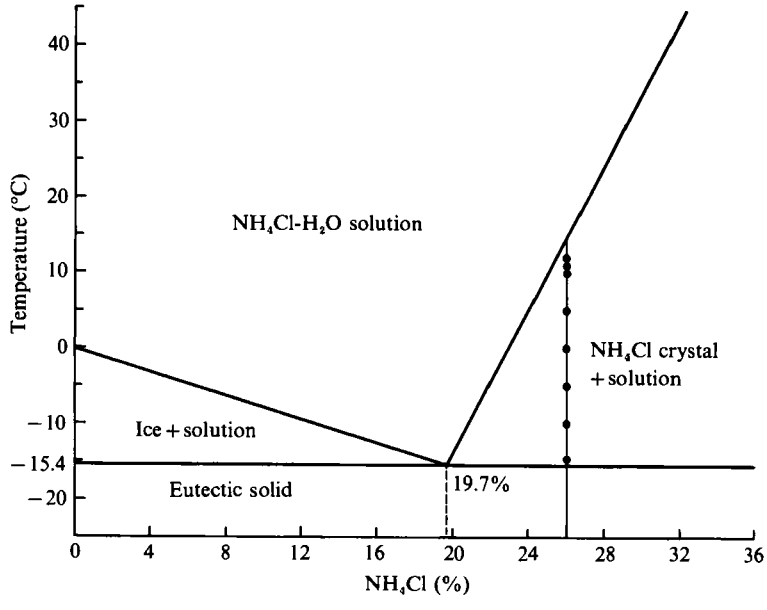

FIGURE 2. Phase diagram of the NH_4Cl-H_2O solution.

presented in table 1. The onset and subsequent evolution of the chimneys depend very much on the cooling temperature of the bottom plate. The experiments conducted can be classified according to the behaviour of chimneys as discussed in §5.2 into three categories: low T_B ($\leqslant -10$ °C), moderate/high T_B (-5 °C to 11 °C), and stable T_B ($= 11.9$ °C). The motion in the bulk fluid in each category is illustrated by a series of shadowgraphs and discussed separately below.

Experiment	T_B (°C)	Onset time (min.)	Mush thickness (cm)
S10	−31.5	24	1.8
S2	−14.3	16	1.1
S11	−14.3	16	0.9
S3	−9.5	20	1.0
S4	−4.4	21	1.0
S5	0.5	25	0.9
S6	5.3	55	1.2
S9	4.3	50	0.8
S7	10.1	89	1.1
S13	11.0	120	0.9
S12	11.9	—	—

TABLE 1. Time of onset of plume convection and thickness of mush at onset. (No records available for S1 and S8.)

3.1. *Low* T_B

This group includes all experiments with $T_B \leqslant -9.5$ °C. In figure 3 (plate 1) we present a series of eight shadowgraphs obtained from experiment S3 with $T_B = -9.5$ °C to illustrate the fluid motion at different stages of the solidification process. The experiment was started at 2.30. By 2.32 (figure 3*a*), crystallization had begun to take place at several spots on the bottom, as evidenced by the lighter fluid being released where crystals had formed. Four minutes later (figure 3*b*), the bottom was completely covered with dendritic crystals, forming a layer of mush 2 mm thick. The rejected fluid at the mush–liquid interface, being cooler and less concentrated than the bulk solution, was being transported upward by salt-finger convection, as seen in the shadowgraph. The warm and more concentrated bulk solution was being transported downward toward the mush by the same finger convection, thus promoting further solidification. The fingers themselves became unstable and degenerated into large-scale convection at approximately 3 to 3 cm. Fully developed finger convection is shown in figure 3(*c*) at 2.40.

At 2.50 (figure 3*d*), several plumes were observed to rise above the finger field, indicating a more buoyant fluid in these plumes. The lighter fluid in the plumes came from the interior of the mushy zone, where the temperature was lower than that at the mush–liquid interface. Crystallization taking place in the mush at these lower temperatures further reduced the concentration of NH_4Cl in the rejected fluid. The buoyant fluid came out of the mushy zone in small chimneys distributed throughout the mush layer. These plumes became stronger as time progressed, as shown in figure 3(*e*) at 3.00. It can be seen from the shadowgraph that finger convection was beginning to fade because the plumes, once started, introduced an additional mechanism to effect mass exchange between the mush layer and the bulk solution. The plume convection became stronger with time, and by 3.30 (figure 3*f*), the fingers had completely disappeared, and the upward convection was carried entirely by the plumes. Although the crystallization process was still taking place at the mush–liquid interface, the residual fluid was returned to the bulk solution by way of the plumes.

From 3.30 to 4.00 (figure 3*f*, *g*), the number of plumes decreased and individual plumes became stronger, reaching heights of between 10 and 12 cm before they became unstable and broke up into general convection. At the exit of each chimney, the upward flow in the plume induced motion of the bulk fluid toward the plume

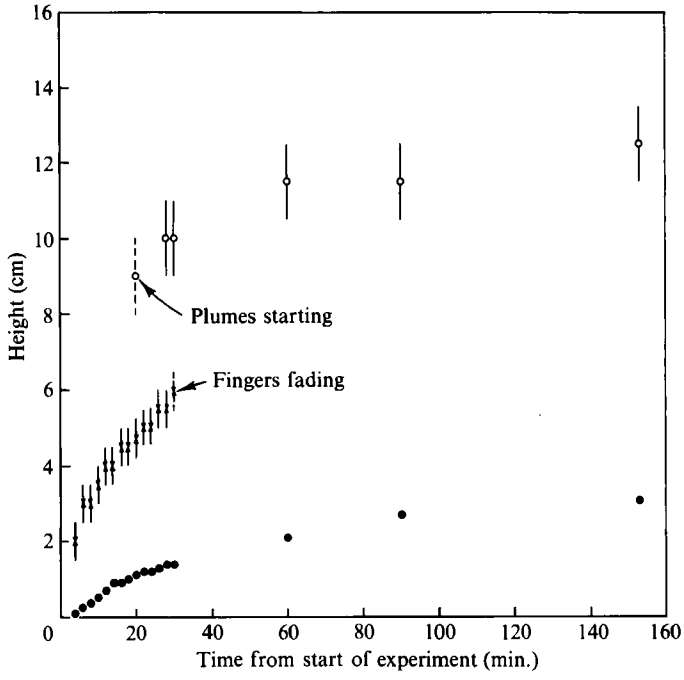

FIGURE 4. Thickness of the mushy zone and heights reached by fingers and plumes for experiment S3 with $T_B = -9.5$ °C. The vertical bars indicate limits of uncertainty. ●, Mushy zone; ⧗, fingers; ○, plumes.

itself. The comparatively solute-rich fluid, meeting the cold plume, tended to crystallize around the chimney. As a result, there was always a buildup of crystals around each chimney exit, not unlike a mini-volcano. These are increasingly evident in the last three shadowgraphs. by comparing shadowgraphs 3(*h*) and 3(*g*), the disappearance of a plume near the right wall is clearly exhibited.

The sequence of events shown in figure 3 is summarized in figure 4, in which the thickness of the mushy zone and the nominal lengths of the fingers and plumes are shown as functions of time. The mushy zone grew linearly with time at first, then the rate of growth decreased steadily. The finger convection started soon after the experiment was initiated, and then it gave way to plume convection in approximately 40 min. In this experiment, the overlap between finger and plume convection was approximately 20 min. As T_B was increased, the overlap region became longer, as discussed below.

3.2. *Moderate/high* T_B

This group consists of six experiments with T_B ranging from −4.4 °C (S4) to 11.0 °C (S13). Plumes appeared in all experiments, even when T_B was only 4 °C below the liquidus temperature. The number of plumes in the early part of the experiment was much smaller than in the low-T_B group. Consequently, the convection due to the plumes was quite weak initially. As a result, the finger convection and the plume convection processes coexisted for approximately 2 to 4 h as T_B was increased. In figure 5 (plate 2) shadowgraphs obtained from experiment S7 with a $T_B = 10.1$ °C are shown. The experiment was started at 10.10. Because of the high T_B, it took 50 min. for the dendrites to cover the tank bottom completely. At 11.30 (figure 5*a*), the fingers were clearly visible. They were very stable because of (i) the comparatively low buoyancy of the fluid rejected by crystallization at relatively high temperatures

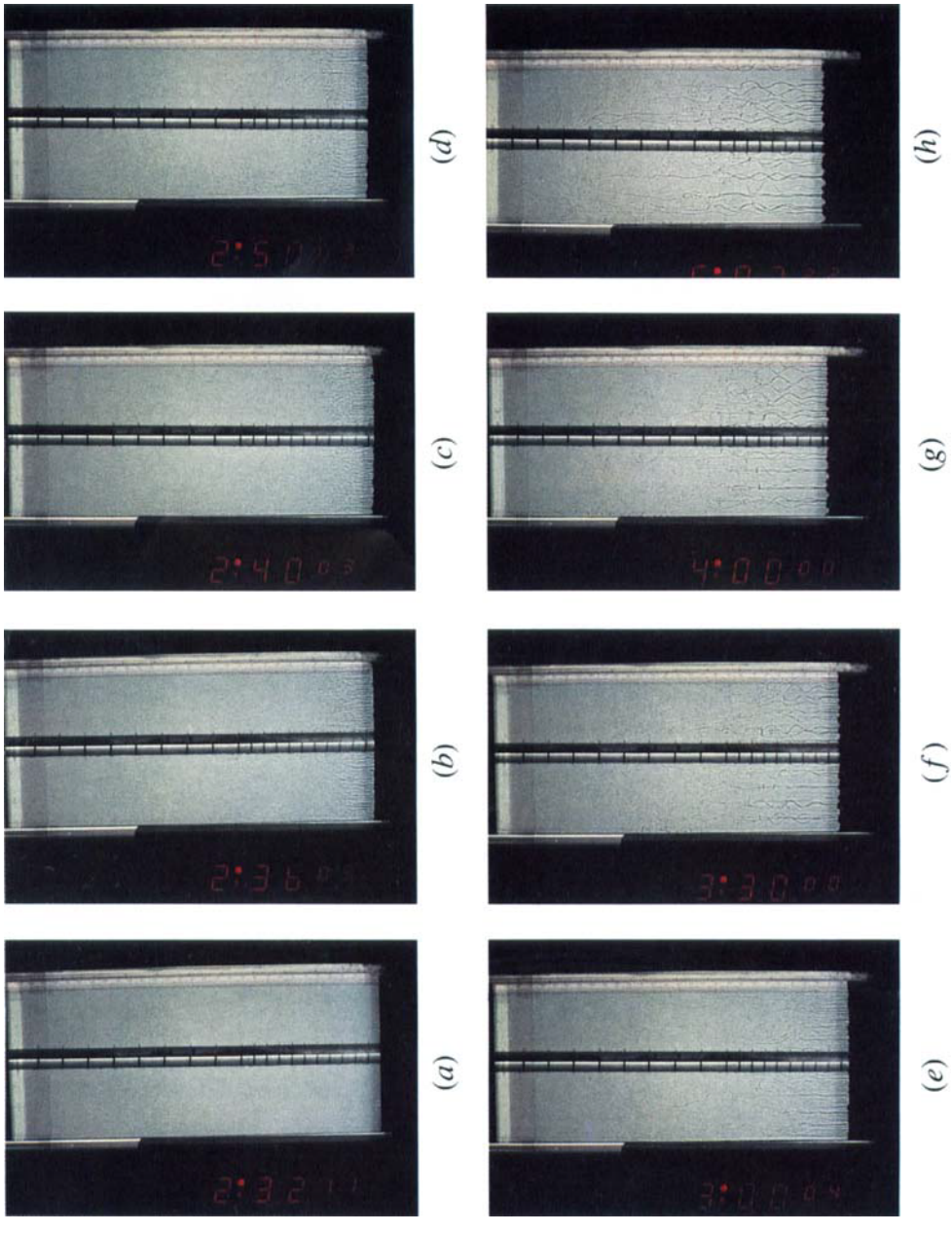

FIGURE 3. Shadowgraphs from experiment S3 with $T_B = -9.5°C$. The experiment was started at 2:30. Initially, the motion was dominated by finger convection above the mush. At 2:50, some plumes can be seen, and they are fully developed at 3:30. Note the disappearance of one plume near the right wall between 4:00 and 5:03. (*a*) Time = 2:32, (*b*) 2:36, (*c*) 2:40, (*d*) 2:50, (*e*) 3:00, (*f*) 3:30, (*g*) 4:00, (*h*) 5:03.

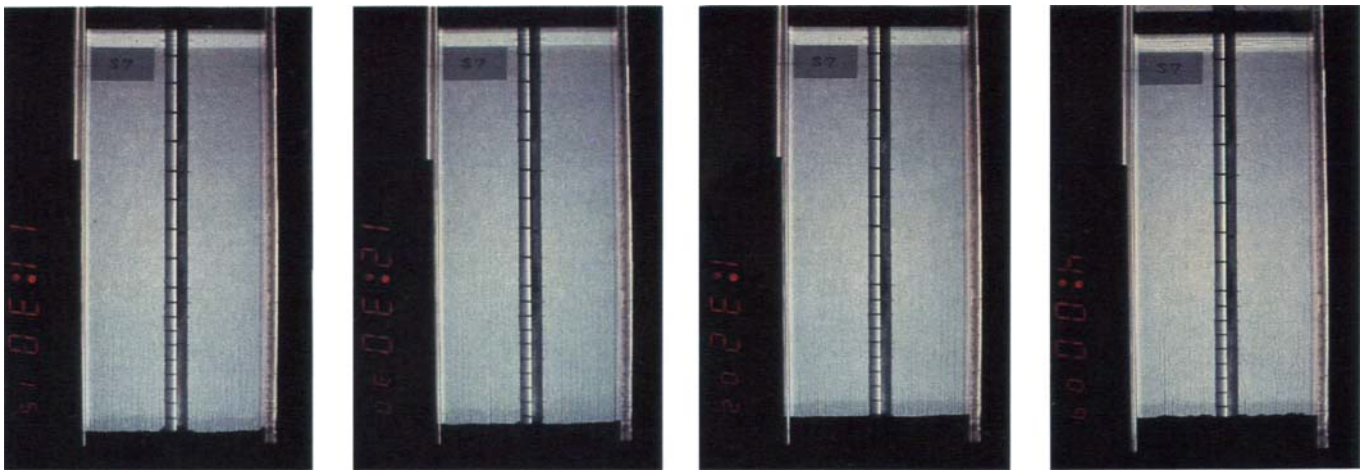

(a) (b) (c) (d)

FIGURE 5. Shadowgraphs from experiment S7 with $T_B = 10.1°C$. Experiment started at 10:12, and it took approximately 50 min. for the dendrites to cover the bottom completely. Finger convection was very stable owing to low buoyancy and the large region with a stable temperature gradient. Simultaneous plume and finger convection occurred for a long time; by 4:00, finger convection had disappeared. (*a*) Time = 11:30, (*b*) 12:30, (*c*) 1:32, (*d*) 4:00.

(a) (b)

FIGURE 6. Structure of the mush. (*a*) S11 with $T_B = -14.3°C$. Note two frozen chimneys on the right. (*b*) S13 with $T_B = 11.0°C$.

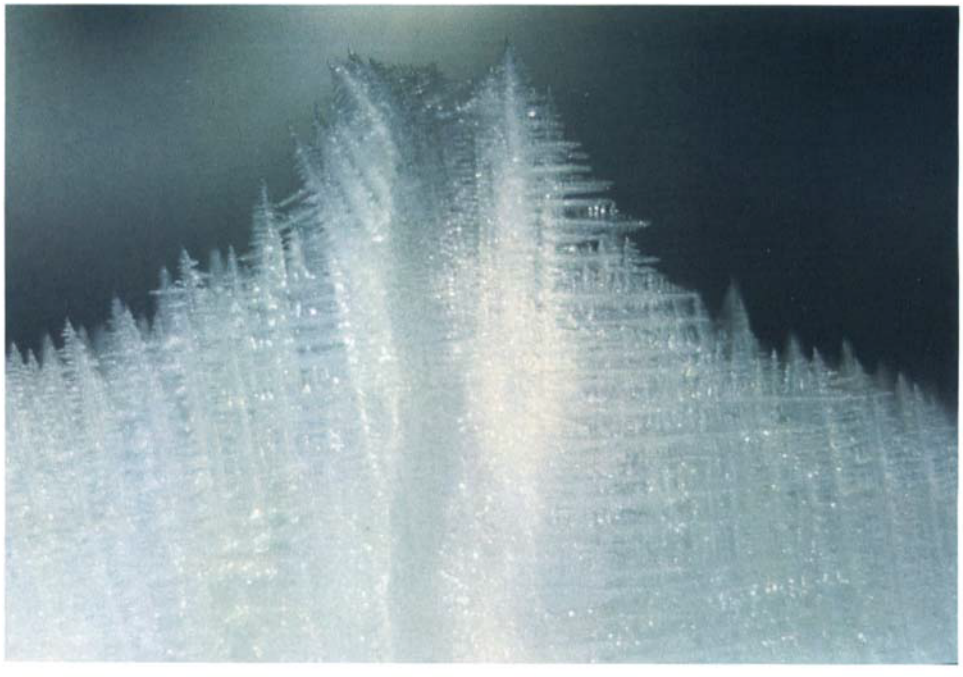

(*a*)

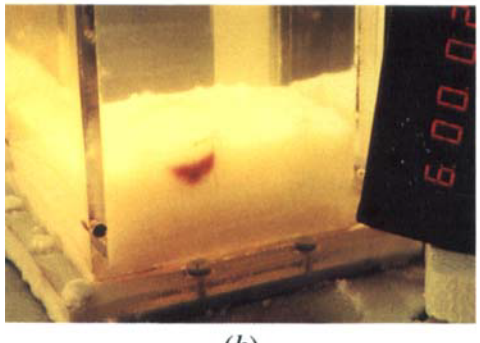

(*b*)

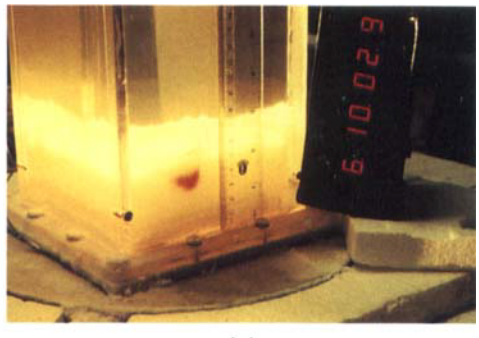

(*c*)

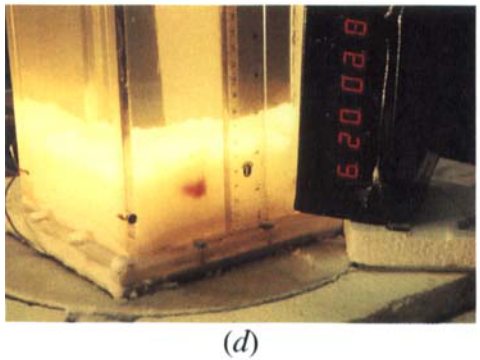

(*d*)

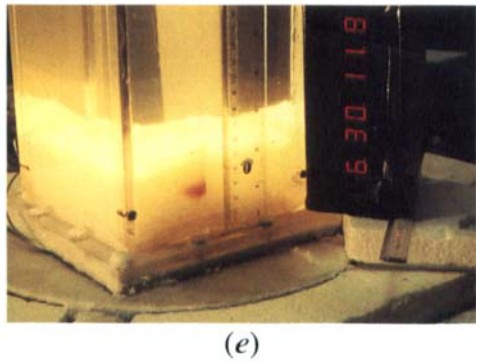

(*e*)

FIGURE 7. (*a*) Close-up view of chimney exit. Photo made by Mark Hallworth of DAMTP. (*b*–*e*) Visualization of flow in the mush. Sequence taken at 10 min. intervals starting 15 min. after the dye had been applied. Experiment was conducted at DAMTP with $T_B \simeq -30°C$. Note eutectic layer at bottom of tank.

and (ii) the extended region with a stable temperature gradient. Plumes and chimneys were first noticed at 11.39, and at 12.30 (figure 5*b*) they were visible in the shadowgraph. At this time, the plumes were remarkably stable, again because of the low buoyancy. At later times, as the mushy zone became thicker and the temperature at a given height of the mushy zone decreased further, buoyancy of the fluid in the plume became large enough to cause spiral instabilities of the plume to occur at lower heights, as shown in figure 5(*c*) at 1.32. It can also be seen that finger convection was getting weaker. By 4.00 (figure 5*d*), convection was entirely due to the plumes. The overlap between finger and plume convection was approximately 4 h.

3.3 *Stable* T_B

With the 26% NH_4Cl-H_2O solution, when the bottom temperature was raised to 11.9 °C, no plumes occurred during the entire experiment S12, which lasted for 13 h. The experiment was started at 9.00, and it took 3 h for the bottom to be entirely covered with dendrites. Stable finger convection persisted throughout the experiment. Copley *et al.* (1970) showed that the plumes can be made to disappear by increasing the thermal gradient. The seemingly contradictory results from their experiments and ours may be due to the difference in the cooling technique. In their experiment, the bottom of the tank was chilled by a flow of liquid nitrogen, and there was a layer of eutectic solid underneath the mush. This means that there is a sink of the lighter liquid at the eutectic–mush interface. The effect of lowering the bottom temperature with increasing flow rate of liquid nitrogen is, we believe, to increase the sink strength, thus reducing the potential for generating plumes.

4. Structure of and flow in the mush

The appearance of the mush as seen through the sidewall of the tank is presented in figure 6 (plate 2) for the low (−14.3%) and high (+11 °C) T_B cases. The mush generally consists of vertical or nearly vertical primary dendrites with secondary and tertiary arms. At the mush–liquid interface, there are usually a number of volcano-like chimney outlets. Figure 7(*a*) (plate 3) shows the mush at $3\frac{1}{2}$ hr into experiment S11 with $T_B = -14.3$ °C. There are four chimneys in view; the two on the right had frozen interiors and the two on the left were still convecting. The second chimney from the right had been frozen some time ago, and a layer of dendrites had grown on top of it. The one on the right had been frozen not very long before the picture was taken. These are the counterparts of the freckles obtained in a Pb-Sn ingot by Sarazin & Hellawell (1988). The slight fuzziness in the lower part of the picture was due to condensation on the wall. Away from the chimneys, the primary dendrites are essentially vertical cylinders. Near the exit of the chimney, the primary dendrites seem to be horizontal, probably due to the large horizontal temperature gradient there. This is more clearly shown in an extreme close-up of a chimney exit made by Mark Hallworth of DAMTP, University of Cambridge, shown in figure 7(*a*). To fix ideas about the scale, the inner diameter of the chimney is 2 mm. Away from the chimney, we see almost vertical primary dendrites with near-horizontal secondary arms. One can almost make out the tertiary arms. Near the chimney, the horizontal primary dendrites are quite prominent.

At high T_B, the dendrites seemed to be a little less tightly packed than in the cases with lower T_B. The dendrites at 11 h into experiment S13 with $T_B = 11.0$ °C are shown in figure 6(*b*). The size of the dendrite arms may be estimated by two available lengthscales in the photo. The centre-to-centre distance between two adjacent screws

is 28 mm, and the upper clear part of the screw hole is 2.5 mm in diameter. By projecting the slide on a piece of paper, tracing the dendrites on the paper, and counting the number within a given distance, the approximate size of the dendrites was found to be 0.5 mm.

The flow field near a chimney in the mush was obtained in an experiment conducted at Cambridge. The 26% NH_4Cl-H_2O solution was cooled from the bottom at a temperature below the eutectic, and the flow visualization study was carried out approximately 6 h into the experiment. The visualization was accomplished by using a deep red dye, which was made by dissolving a very small amount of potassium permanganate crystals into a NH_4Cl solution withdrawn near the mush–fluid interface of the tank. In this manner, we tried to keep any density variations between the dye solution and fluid near the mush to a minimum. The dye solution was carefully placed on top of the mush layer near a chimney in a horizontal patch approximately 2 cm in width. The motion of the dye is illustrated by the sequence of four photos taken at 10 min. intervals shown in figure 7(*b–e*) (plate 3). Since the bottom temperature was kept lower than the eutectic temperature, a eutectic layer at the bottom of the tank was clearly visible. All chimneys ended at the mush–eutectic interface. Figure 7(*b*) shows the position of the dye patch approximately 15 min. after the dye had been applied. Ten minutes later (figure 7*c*), the dye patch was drawn downward, as well as towards the right, into the chimney. At 6.20 (figure 7*d*), the dye patch had become weaker because part of the dye solution had been entrained into the plume, as evidenced by the faint red trace in the plume. This effect is more pronounced at 6:30, as shown in figure 7(*e*). From the complete series of photos, of which only four are shown here, we estimated the average descending velocity of the fluid in the mush to be 0.35 mm/min. It is also evident that the outer boundary of the dyed region is approximately a parabola.

5. Onset and evolution of chimneys and plumes

5.1. *Onset of Plume Convection*

the time of onset of plume convection with concomitant surfacing of chimneys for each of the experiments is listed in table 1, together with the thickness of the mushy zone at the time of onset. These are graphed in figure 8. The time of onset increased linearly with time from $T_B = -15$ °C to $T_B = 0$ °C, then it increases with a much larger slope to $T_B = 11$ °C. The thickness of the mushy zone is, however, almost a constant at 1 cm. The cross in each graph denotes the data from the experiment with $T_B = -31.5$ °C, below the eutectic temperature, showing the combined thickness of the eutectic and mush layers to be 1.8 cm. Data taken 14 min. later show that the mush and the eutectic layers were of equal thickness. Assuming the same holds true at the time of onset, then the mush thickness would be 0.9 cm (denoted by a triangle), consistent with the rest of the data. The nearly constant thickness of the mushy layer at the time of onset of plume convection is a remarkable result, especially in view of the fact that the temperature difference across the mush layer ranged from 4 °C to 30 °C in these experiments.

5.2. *Time evolution of chimneys*

The number of chimneys always changed during the course of each experiment. The characteristics of the time variation of the number of chimneys for the low-T_B group are very different from those of the moderate/high-T_B group. These are shown by three representative cases in figure 9. The low-T_B group is represented by experiment

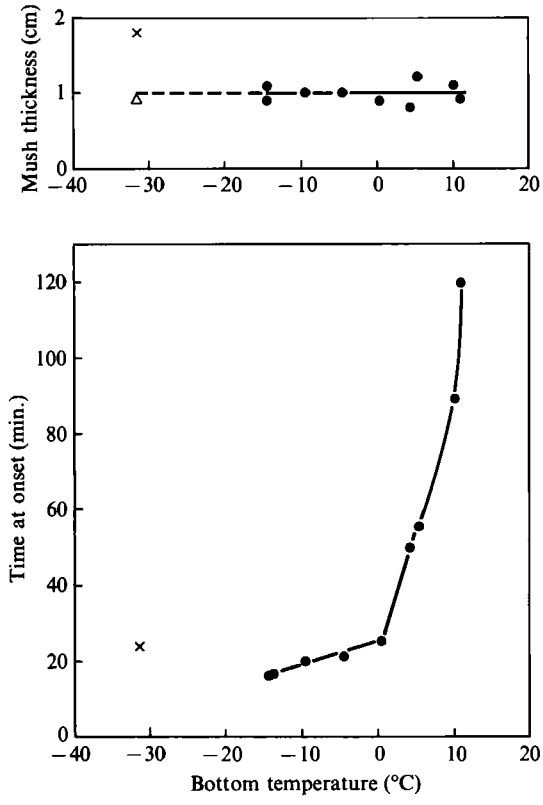

FIGURE 8. Time of onset of plume convection and thickness of mushy zone at onset.

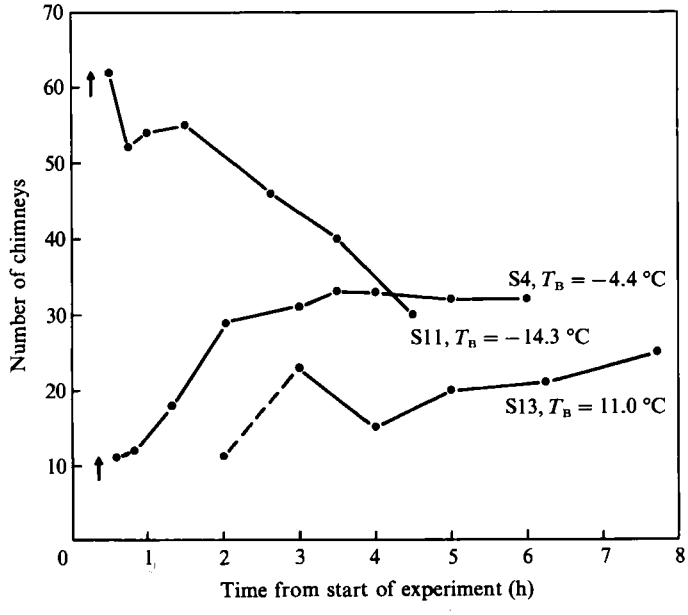

FIGURE 9. Time evolution of the number of chimneys at three different T_B values.

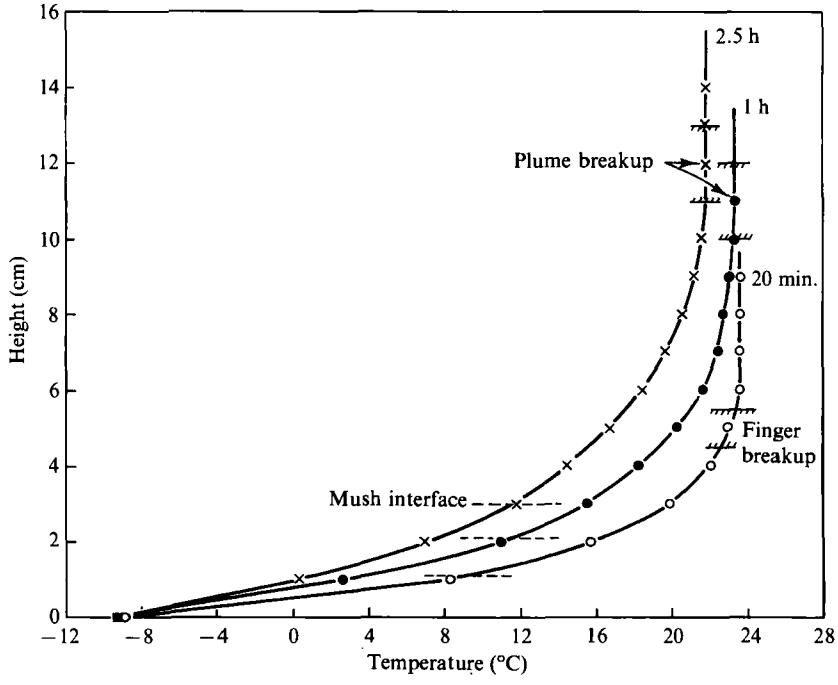

FIGURE 10. Temperature distributions near the bottom of the tank at three different times for experiment S3. ---, location of mush–liquid interface.

S11 with $T_B = -14.3$ °C. A large number of chimneys, 60–70, appeared shortly after onset. The cross-sectional area of these chimneys is rather small. The number of chimneys gradually decreased until the end of the experiment, while the cross-sectional area of the chimneys increased.

The moderate/high-T_B group is represented by two cases, S4 and S13. In experiment S4 with $T_B = -4.4$ °C, the initial number of chimneys, 10–20, was considerably smaller than for the low-T_B group. The number subsequently increased to a plateau of approximately 35, then slowly decreased. In experiment S13 with $T_B = 11.0$ °C, the growth curve is shifted about $1\frac{1}{2}$ h later with respect to that for S4. We note that for this experiment, it took 3 h for the dendrites to cover the bottom completely. The first data point was obtained 2 h into the experiment and there were 11 plumes from regions covered by dendrites. The points at 2 h and 3 h are connected by a dashed line.

6. Temperature distribution

Temperatures at selected points in the fluid and in the mush, were recorded at intervals for all experiments. Such distributions are shown for experiment S3 in figure 10 at 20 min., 1 h, and 2 h 30 min. into the experiment. The position of the mush–liquid interface and the locations of the breakup of the fingers and plumes are indicated on the graph. The initial fluid temperature was 23.6 °C. At 20 min. the mush was 1.1 cm thick and the fingers broke up just below the point where the fluid temperature became constant. A shadowgraph of the flow is shown in figure 3(*d*) at 2.50. At 1 h into this experiment, the mushy zone grew to 2.1 cm thick and the plumes broke up where the fluid temperature became constant, similar to the case with finger convection. A shadowgraph at this time, 3.30, is shown in figure 3(*f*). At

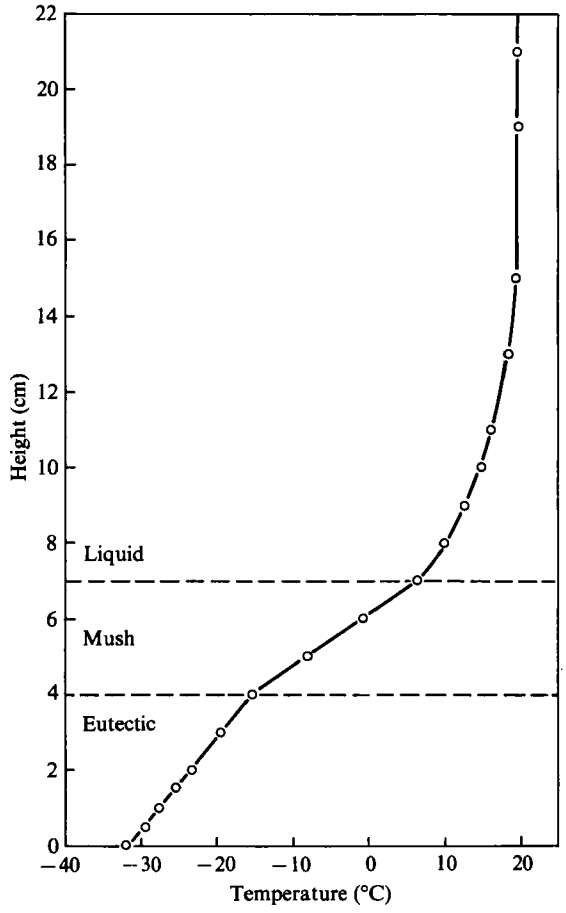

FIGURE 11. Temperature distribution through the liquid, mush, and eutectic layers for experiment S10 with $T_B = -31.5$ °C at 6 h 29 min. into the experiment.

2 h 30 min. into the experiment, the fluid in the tank had been cooled by about 2 °C. The mush continued to grow and the temperature of the mush at a given height became lower as the solidification process proceeded. A shadowgraph at this time is shown in figure 3(*h*). The temperature at the interface at 20 min. was 9.1 °C, considerably lower than the liquidus temperature of 15 °C.

The temperature distribution through the eutectic and mush layers is shown in figure 11 for experiment S10 with $T_B = -31.5$ °C. The data presented were taken 6 h 29 min. into the experiment, when the eutectic layer was 4 cm thick and the mush layer was 3 cm thick. The temperature distribution was linear in both layers, and the temperature at the interface between the two layers was at the eutectic temperature of −15.4 °C. At this time, the number of chimneys had decreased to 41 and the convection was not very vigorous.

7. Probing the mushy zone by computed tomography

In order to fully understand the fluid motion in the mushy zone, we must have more knowledge about the physical properties of the mush. This is a rather difficult task because the dendritic structure is very fragile. When fluid is drained out of the

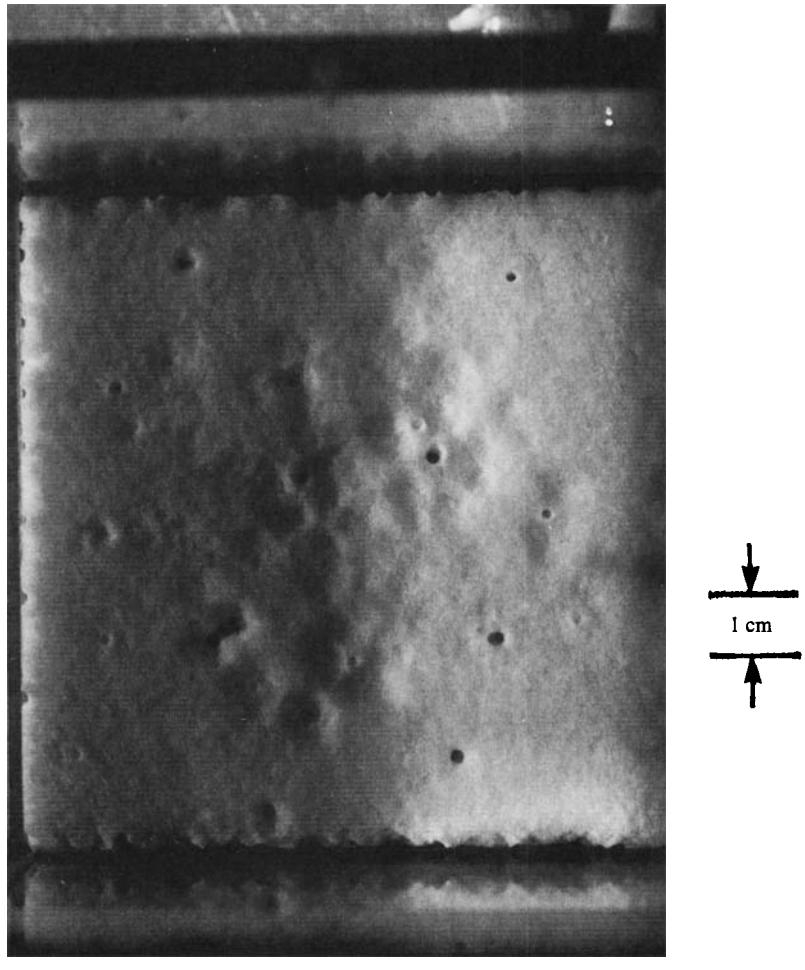

FIGURE 12. Top view of the mushy zone to be scanned by computed tomography. The 1 cm region scanned is indicated in the figure.

mush, it slumps somewhat because the fluid contributes to its support. Therefore, it is important to examine the mushy zone with the saturating fluid in place. The computed tomography technique, widely used in the field of medicine, may provide a way to measure some physical properties of the mush.

Computed tomography is a well-developed technique for medical diagnostic applications; see Sprawls (1987) for an introduction to this technique. Its basis is that the X-ray attenuation coefficient of an element is proportional to the third power of the atomic number of the element, regardless of its chemical or physical state. A patient being examined in a CT scanner is being radiated by a perpendicular sheet of X-rays 2 to 4 mm in thickness. By rotating the source of the X-rays and the receptor array in a complete circle, each part of the body within the slice is examined from a number of different angles and the cumulative attenuation effect is recorded in a computer. By the application of suitable inversion software, the X-ray attenuation coefficient of each small area in the cross-section of the body can be obtained and converted into an image intensity. The result is a CT image of that slice of the body.

Recently, research engineers and scientists in the petroleum industry have applied this technique to determine the characteristics of core samples of rocks (Withjack 1987) and to visualize fluid flow through a porous medium (Withjack & Akervoll 1988). We recently carried out a preliminary experiment with the collaboration of Dr Evan Unger, Director of CT and MRI, Arizona Health Sciences Center, University of Arizona. The results are most encouraging and are summarized below.

7.1. *Photos from a CT scan*

To facilitate the movement of the test tank through the CT scanner, a tank of smaller height was constructed. It was a cube, 12.7 cm on all sides, made of Plexiglas. In order to obtain a sizeable mushy zone, a higher concentration, 30% NH_4Cl-H_2O solution was used. A directional solidification experiment was first carried out. The growth of the mushy zone and then later the onset and maintenance of upward-flowing plumes through chimneys were observed. The experiment was terminated approximately $1\frac{1}{2}$ h after the start, and the mushy zone was approximately 3 cm thick. The scanning was carried out 2 days later. At that time, all convection had ceased. The liquidus temperature of a 30 wt% NH_4Cl-H_2O solution is 31 °C, approximately 6 °C above the temperature in the laboratory. Furthermore, dissolving NH_4Cl is an endothermic process requiring 3.533 kcal/mole or 66.7 cal/g at 25 °C (Weast 1974), and there was minimal remelting on the global scale taking place over the 2-day period. (We remark here that in order to reuse the solution in the experiments, the fluid had to be vigorously stirred so that the NH_4Cl crystals would go into solution.) During the 2-day period, there might have been some internal adjustment of the solid fraction across the layer, and the volcanic sprouts at the chimneys all remelted into the solution because of their exposed positions. A photo of the top view of the tank, taken before the CT scan, is shown in figure 12. There were 10 chimneys in the main body of the mushy zone. The 1 cm thick region surveyed by the CT scanner is indicated in the figure.

The thickness of the X-ray was set at 2 mm. After each scan, the table was advanced 2 mm for the next scan. The procedure was repeated six times, covering a horizontal distance of 1 cm. Six photos are shown in sequence in figure 13; these are negatives in which dark areas denote less attenuation and white areas, more attenuation. Figure 13(*a*) shows a slice of the mushy zone more or less free of chimneys, although there is one on the left which is faintly visible. Figure 13(*b*) shows the presence of two chimneys, one on the left and the other on the right, together with the root section of a chimney in between the two. In figure 13(*c*), there is a large chimney on the left side of the tank, which is an amalgamation of two separate ones. Figure 13(*d*) shows the viewing plane cutting right through two large chimneys and one smaller one on the extreme left. In figure 13(*e*), the plane is cutting through the peripheral regions of four chimneys. The last photo in this sequence, figure 13(*f*), shows a small chimney in the centre of the tank. We note here that the edges of the chimneys show higher X-ray attenuation. This is corroborated by the close-up photo of a chimney shown in figure 7(*a*), in which the rim of the chimney was shown to be more tightly packed with dendrites. Further, these photos show that the interior chimneys, like the ones near the wall, have large root sections.

7.2. *Porosity of the mush*

Besides giving us a visual image of the mushy zone including the chimneys, the CT scanner will yield, in a digital output, the linear attenuation coefficient in Hounsfield units for each voxel in the viewing area. One Hounsfield (*H*), more commonly known

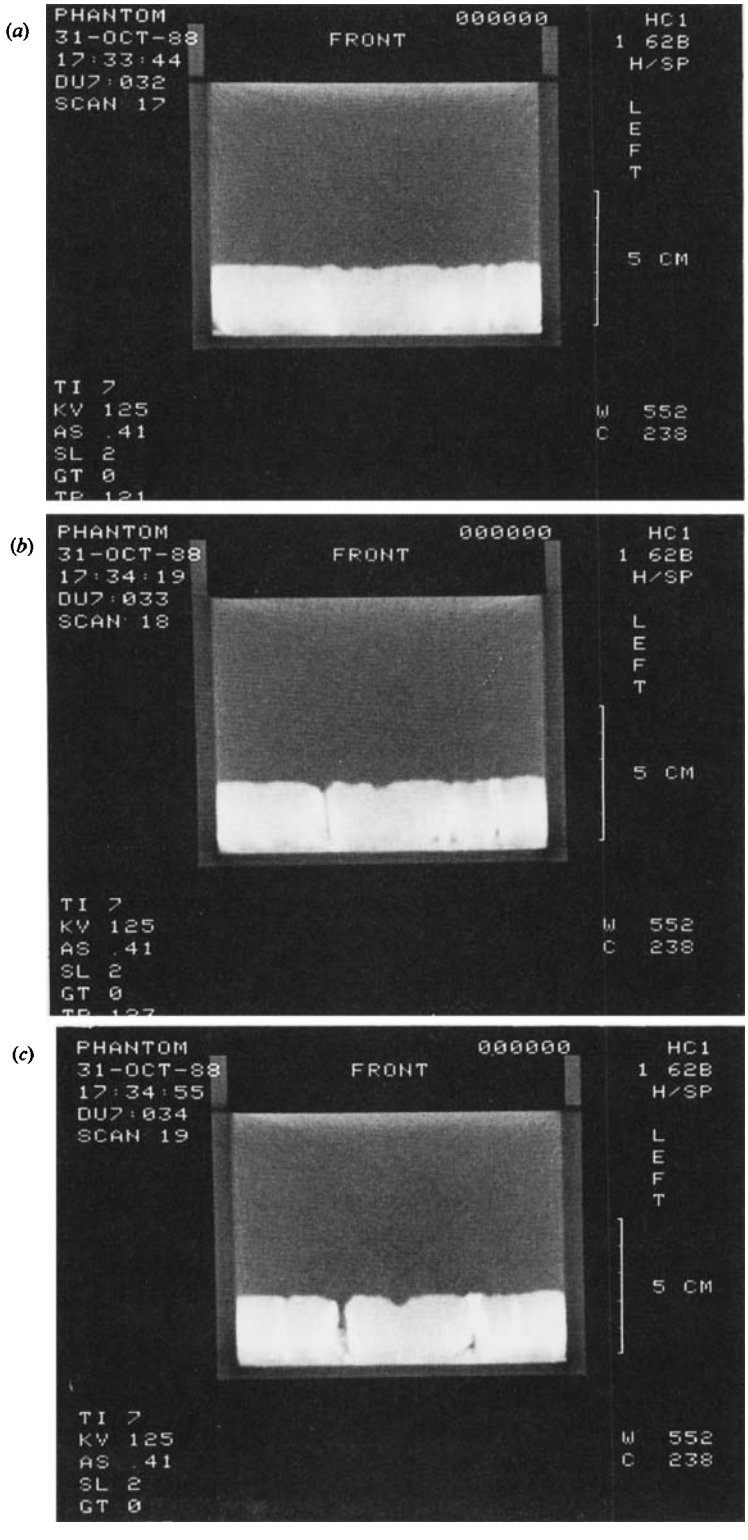

FIGURE 13 (*a–c*). For caption see facing page.

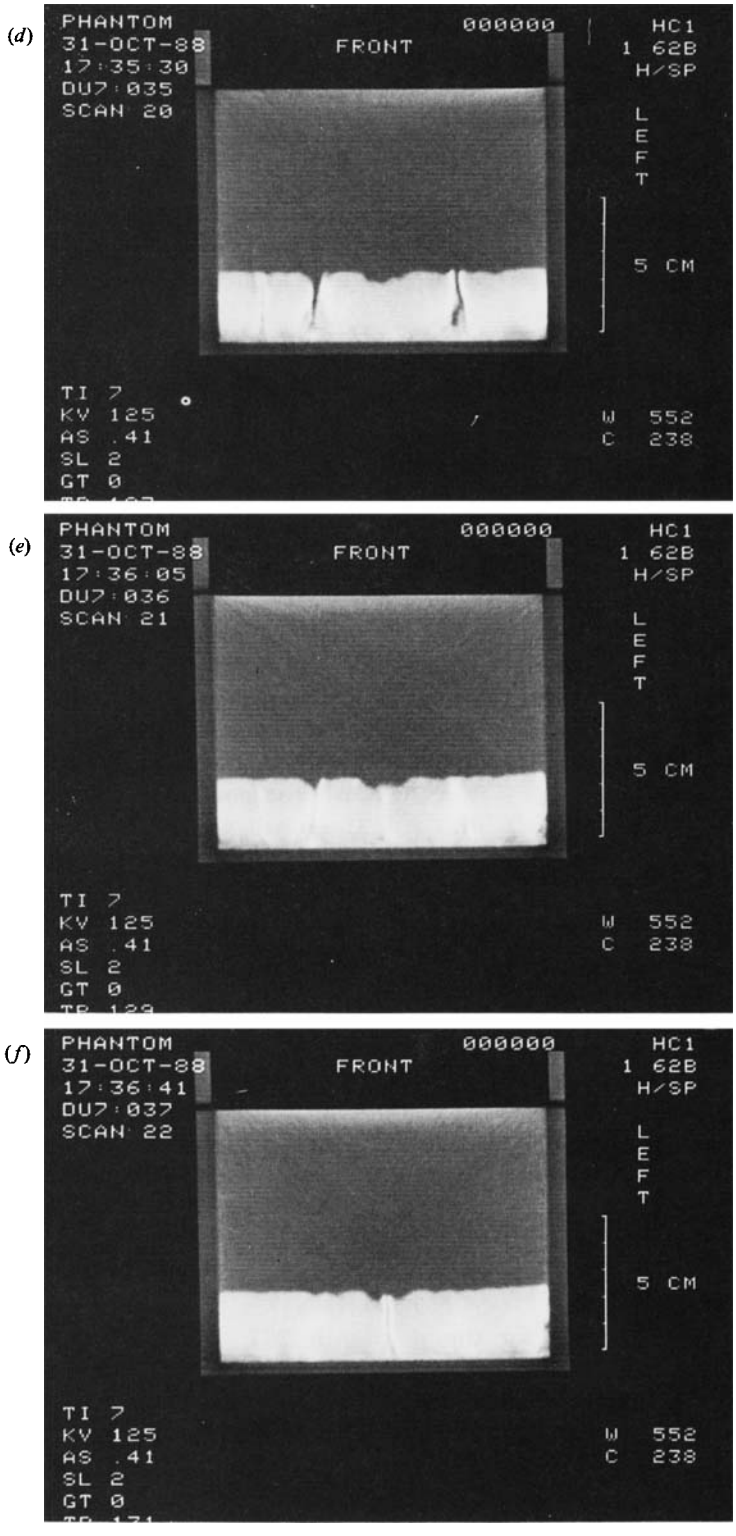

FIGURE 13. Computed tomography images of the mushy zone. The thickness of the X-ray was 2 mm, and the table was advanced 2 mm after each scan. These six photos cover a 1 cm slice of the mushy zone.

as the CT number, represents 0.1 % of the attenuation coefficients of water, which is also chosen as the datum of the scale; i.e. H (water) = 0. For any specimen, H is related to the attenuation coefficient μ by the following expression (Barrett 1981):

$$H = \frac{\mu\,(\text{specimen}) - \mu\,(\text{water})}{\mu\,(\text{water})} \times 1000 = \text{CT number}.$$

In our experiment, each voxel measures approximately $1 \times 1 \times 2$ mm thick. For each voxel, the attenuation coefficient was known. If the porosity of the mush within each voxel is ϵ, then the value μ as measured can be expressed as

$$\mu = \epsilon\mu_{\mathrm{f}} + (1-\epsilon)\,\mu_{\mathrm{s}},$$

in which μ_{f} and μ_{s} denote the attenuation coefficient of the NH_4Cl-H_2O solution and the NH_4Cl crystal, respectively. The values of μ_{f} and μ_{s} can be obtained by calibration. This expression can be easily derived from the relationship between the attenuation coefficient of a mixture of different components and that of each component of the mixture (Barrett 1981):

$$\frac{\mu_{\mathrm{m}}}{\rho_{\mathrm{m}}} = \sum_{i=1}^{I} \left(\frac{\mu}{\rho}\right)_i W_i.$$

In the above equation, ρ is the density, W is the weight fraction, and subscripts m and i denote the mixture and ith component, respectively.

A survey of the X-ray attenuation coefficient in the liquid and the mushy zone in a region free of chimneys was made in a subsequent test with the same solution. The CT scan was carried out one day after the mush was generated. The results are shown in figure 14(*b*). Here, the distribution in the mush was sketched in with a sharp transition at the interface and ignoring the low reading at the bottom. (This reading may be erroneous owing to the extremely low CT number of the Plexiglas.) The exact distribution can be obtained by recording the CT number at closer intervals. The present approximation is more than adequate to examine the feasibility of the technique.

The fluid in the mushy zone will have concentrations different from that of the bulk fluid. For this preliminary study, however, we assume a constant CT number of 200 for the fluid in the mush. To obtain the value of μ_{s}, we scanned the NH_4Cl powder contained in the same Plexiglas tank. Since air is essentially transparent to X-rays and the weight fraction of NH_4Cl powder is nearly 1, the attenuation coefficient of NH_4Cl, μ_{s}, can be approximated by

$$\mu_{\mathrm{s}} = \frac{\mu_{\mathrm{m}}\rho_{\mathrm{s}}}{\rho_{\mathrm{m}}}$$

with good accuracy.

The average CT reading for the powder is 377. With $\rho_{\mathrm{s}} = 1.5256\ \mathrm{g/cm^3}$ and $\rho_{\mathrm{m}} = 0.85\ \mathrm{g/cm^3}$, the CT number for a NH_4Cl solid is 677. The porosity ϵ of the mush evaluated using these values are shown in figure 14(*a*). It is seen that the porosity of the mush is between 0.6 and 0.65 and decreases toward the bottom, indicating more solidification there. With the porosity value known, the critical Rayleigh number for the onset of plume convection can be estimated. We note here that had we scanned the mush layer immediately at the end of the experiment, the porosity distribution may have shown a different gradient.

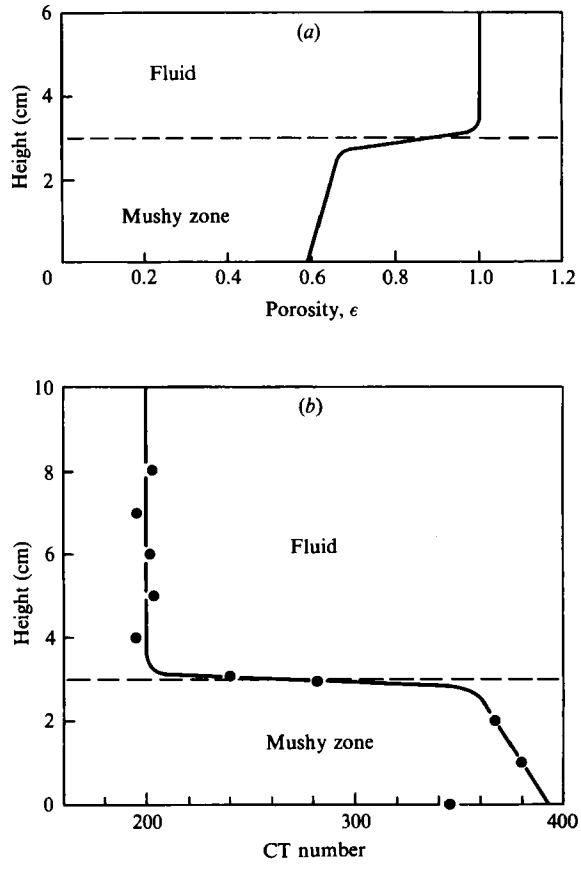

FIGURE 14. (*a*) Porosity and (*b*) CT number in the mushy zone.

7.3. *Estimate of the critical Rayleigh number for the onset of plume convection*

The critical condition can be expressed as when the equivalent Rayleigh number exceeds a certain limit:

$$R_{\rm eq} = R_S - R_T > R_{\rm C},$$

in which the thermal and solute Rayleigh numbers are appropriately defined for a porous layer:

$$R_T = \frac{g\alpha\Delta TKD}{\kappa^*\nu} \quad \text{and} \quad R_S = \frac{g\beta\Delta SKD}{\kappa_S'\nu}.$$

In the above expressions, g is the gravitational acceleration, $\alpha = -\rho^{-1}(\partial\rho/\partial T)_S$, ΔT is the temperature difference across the porous layer, K is the permeability, D is the thickness of the layer, ν is the kinematic viscosity, and κ^* is a thermal diffusivity appropriate for the porous layer and is defined as the thermal conductivity of the porous medium divided by the heat capacity of the fluid, $k_{\rm m}/(\rho C)_{\rm f}$. For the solute Rayleigh number R_S, $\beta = \rho^{-1}(\partial\rho/\partial S)_T$, ΔS is the concentration difference across the layer, and κ_S' is the solute diffusivity in the porous medium. It is noted that $\kappa_S'/\kappa^* \approx 10^{-2}$ and R_T may be neglected compared to R_S.

The value of permeability K can be obtained by using the Kozeny–Carman equation (Beckermann & Viskanta 1988),

$$K = \frac{\epsilon^3 d^2}{180\,(1-\epsilon)^2},$$

Experiment	T_B (°C)	Plume convection	ΔS (%)	R_S
S11	−14.3	Vigorous	4.5	2231
S13	+11.0	Slow	0.5	248
S12	+11.9	None	0.4	198

TABLE 2. Computed values of R_S for three experiments.

where d is the base diameter of a slender cone approximating the dendrite. Even though this relationship was developed for packed spheres, correlations very similar in form to the Kozeny–Carman equation are recommended by Poirier (1987) based on a number of experimental results for Pb-Sn and borneol-paraffin alloys. Using a mean value of $\epsilon = 0.625$ and $d = 0.05$ cm, we obtain $K = 2.41 \times 10^{-5}$ cm^2.

We shall now apply this permeability value for the evaluation of R_S for several experiments reported here. Even though the scanned sample was from a 30 wt% solution and scanning was performed one day after the solidification experiment, it is our belief that the porosity value is representative of the mush layers generated in our experiments. This is because the relatively high liquidus temperature of the solution and the large heat of solution of NH_4Cl permitted negligible amounts of remelting. Furthermore, the structure of the mush in the sample did not differ in any significant way from those we observed in our experiments. For the evaluation of R_S, the other property values are: $\beta = 2.82 \times 10^{-3}$ %$^{-1}$, $D = 1$ cm, $\kappa'_S = 1.12 \times 10^{-5}$ cm^{-5}/s, $\nu = 1.2 \times 10^{-2}$ cm^2/s.

It is noted that the diffusivity of NH_4Cl given by the International Critical Table is 1.7×10^{-5} cm^2/S. For a porous medium consisting of 1 mm spheres, Wooding (1959) experimentally determined that the diffusivity of salt is reduced by a factor of 0.66. We have applied that factor to obtain the values listed above. Using these values, we compute R_S for three experiments in which the plume convection was very vigorous, just above the critical condition, and just below the critical condition; and the results are shown in table 2. For S11 and S13, R_S is evaluated at onset of plume convection. The concentration difference ΔS is obtained by knowing the temperatures at the tank bottom and at the mush–liquid interface, and using the liquidus line of the phase diagram to relate the temperature to the concentration. We remark here that for the experiments with T_B between −14.3 and +11.0 °C, $R_S > 248$.

It is seen that the critical Rayleigh number lies between 200 and 250. This set of preliminary values will undoubtedly be refined when the mushy zone can be scanned during the solidification process. It is expected that the same critical R_S range applies to NH_4Cl solution at different concentrations. Experimental confirmation of this result will be carried out in the near future.

8. Effect of reduced gravity

Since both the finger convection phenomenon and the freckling phenomenon (these are two distinct phenomena commonly mistaken to be the same) are gravity driven, directional solidification carried out in a microgravity environment would probably result in castings free of freckles. To test this theory, such an experiment is being planned for a forthcoming space shuttle mission. In preparation for this mission, a similar experiment has been flow in KC-135 missions. Video recordings of

interferometer observations during reduced-gravity manoeuvres show the profound effect of gravity on the entire process (T. D. McCay & M. H. McCay 1988, personal communication).

It is of interest to estimate the level of reduced gravity at which plume convection and finger convection may still occur. It is seen that, at normal gravity, plume convection occurred at a concentration difference across the mush layer of 0.5 wt%. When the solution is cooled rapidly with very low bottom temperatures, the potential difference in concentration across the mush layer is 6% for the 26% NH_4Cl-H_2O solution. It is reasonable to expect that plume convection could occur at $(0.5/6)g$ or $10^{-1}\,g$. We are assuming that the growth of the mushy zone is not materially affected by the reduced gravity. This is a reasonable assumption since the growth of dendrites is due to a morphological instability independent of gravitational effects.

For the onset of finger convection in a fluid layer with free–free boundary conditions, the solute Rayleigh number for the fluid is $R_{fS} \sim 27\pi^4/4$ (Stern 1960). This Rayleigh number is defined as

$$R_{fS} = \frac{g\beta\Delta S H^3}{\kappa_S \nu},$$

in which H is the fluid layer thickness and κ_S is the diffusivity of the solute in the fluid. All other symbols are as defined earlier. Assuming a modest 1% concentration difference between the top of the mush and the bulk fluid, finger convection could occur at $10^{-4}\,g$. If directional solidification of NH_4Cl-H_2O is carried out at a gravity level between $10^{-1}\,g$ and $10^{-4}\,g$, the resulting solid should be free of freckles and, at the same time, the solidification will proceed at a fairly fast rate because of finger convection. It is reasonable to expect that such limits can also be established for metallic alloys.

This series of experiments was started in the Fall of 1987 when C.F.C. was on sabbatical at DAMTP, University of Cambridge. The hospitality of Dr. Herbert Huppert, by letting C.F.C. loose in his laboratory, is greatly appreciated, as is the assistance of Dr Grae Worster and Mr Mark Hallworth. The experiments were continued at the AME Department, University of Arizona, with the financial support of the National Science Foundation under Grant MSM-8702732 and NASA under Grant NAG 3 723, for which we are grateful. We are also grateful for the assistance of Dr Evan Unger, Dr Art Gmitro, and Ms Roxanne George of the Arizona Health Sciences Center in performing the CT scans.

REFERENCES

Barrett, H. H. 1981 *Radiological Imaging*, pp. 334, 376. Academic.

Beckermann, C. & Viskanta, R. 1988 Double-diffusive convection during dendritic solidification of a binary mixture. *PhysicoChem. Hydrodyn.* **10**, 195–213.

Bennon, W. D. & Incropera, F. P. 1987 A continuum model for momentum, heat and species transport in binary solid–liquid phase change systems: II. Application to solidification in a rectangular boundary. *Int. J. Heat Mass Transfer* **30**, 2171–2187.

Copley, S. M., Giamei, A. F., Johnson, S. M. & Hornbecker, M. F. 1970 The origin of freckles in unidirectionally solidified castings. *Metall. Trans.* **1**, 2193–2204.

Fisher, K. M. 1981 The effects of fluid flow on the solidification of industrial castings and ingots. *PhysicoChem. Hydrodyn.* **2**, 311–326.

Fowler, A. G. 1985 The formation of freckles in binary alloys. *IMA J. Appl. Maths* **35**, 159–174.

GIAMEI, A. F. & KEAR, B. H. 1970 On the nature of freckles in nickel-base superalloys. *Metall. Trans.* **1**, 2185–2192.

GLICKSMAN, M. E., CORIELL, S. R. & MCFADDEN, G. B. 1986 Interaction of flows with crystal–melt interface. *Ann. Rev. Fluid Mech.* **18**, 307–335.

HEINRICH, J. C. 1988 Numerical simulations of thermosolutal instability during directional solidification of a binary alloy. *Comput. Meth. Appl. Mech. Engng* **69**, 65–88.

HILLS, R. N., LOPER, D. E. & ROBERTS, P. H. 1983 A thermodynamically consistent model of the mushy zone. *Q. J. Mech. Appl. Maths* **36**, 505–539.

HUPPERT, H. E. & WORSTER, M. G. 1985 Dynamic solidification of a binary alloy. *Nature* **314**, 703–707.

JACKSON, K. A., HUNT, J. D., UHLMANN, D. R. & SEWARD, T. P. 1966 On the origin of the equiaxed zone in castings. *Trans. Metall. Soc. AIME* **236**, 149–158.

KEAR, B. H. 1986 Advanced metals. *Sci. Am.* **255**, 159–167.

MCDONALD, R. J. & HUNT, J. D. 1969 Fluid motion through the partially solid regions of a casting and its importance in understanding A-type segregation. *Trans. Metall. Soc. AIME* **245**, 1993–1996.

MCDONALD, R. J. & HUNT, J. D. 1970 Convective fluid motion within the interdendritic liquid of a casting. *Metall. Trans.* 1, 1787–1788.

MCLEAN, M. 1983 *Directionally Solidified Materials for High Temperature Service*. London: The Metals Society.

MULLINS, W. W. & SEKERKA, R. F. 1964 Stability of a planar interface during solidification of a dilute binary alloy. *J. Appl. Phys.* **35**, 444–451.

POIRIER, D. R. 1987 Permeability to flow of interdendritic liquid in columnar-dendritic alloys. *Metall. Trans.* B **18**, 245–255.

ROBERTS, P. H. & LOPER, D. E. 1983 Toward a theory of the structure and evolution of a dendrite layer. In *Stellar and Planetary Magnetism* (ed. A. M. Soward), pp. 329–349. Gordon and Breach.

SAMPLE, A. K. & HELLAWELL, A. 1984 The mechanism of formation and prevention of channel segregation during alloy solidification. *Metall. Trans.* A **15**, 2163–2173.

SARAZIN, J. R. & HELLAWELL, A. 1988 Channel formation in Pb-Sn, Pb-Sb and Pb-Sn-Sb alloy ingots and comparison with the system NH_4Cl-H_2O. *Metall. Trans.* A **19**, 1861–1871.

SPRAWLS, P. 1987 *Physical Principles of Medical Imaging*. Frederick, MD: Aspen.

STERN, M. E. 1960 The 'salt fountain' and thermohaline convection. *Tellus* **12**, 172–175.

WEAST, R. C. 1974 *Handbook of Chemistry and Physics*, p. D-81. CRC Press.

WITHJACK, E. M. 1987 Computed tomography for work-property determination and fluid-flow visualization. *SPE*-16951. Soc. Petrol. Engrs.

WITHJACK, E. M. & AKERVOLL, A. 1988 Computer tomography studies of 3-D miscible displacement behavior in a laboratory five-spot model, SPE-18096, Soc. Petrol. Engrs.

WOODING, R. A. 1959 The stability of a viscous liquid in a vertical tube containing porous materials. *Proc. R. Soc. Lond.* A **252**, 120–134.

WORSTER, M. G. 1986 Solidification of an alloy from a cooled boundary. *J. Fluid Mech.* **167**, 481–501.